JOURNAL OF BIOMEDICAL OPTICS 3(2), 137–144 (APRIL 1998)

DEPENDENCE OF IMAGE QUALITY ON IMAGE OPERATOR AND NOISE FOR OPTICAL DIFFUSION TOMOGRAPHY

Jenghwa Chang,[†] Harry L. Graber,[‡] and Randall L. Barbour[‡]*
[†]Memorial Sloan-Kettering Cancer Center, Department of Medical Physics, New York, New York 10021; SUNY Health Science Center at Brooklyn, [‡]Program in Physiology and Biophysics, and *Department of Pathology, Brooklyn, New York 11203

(Paper JBO-105 received Sep. 24, 1996; revised manuscript received Oct. 15, 1997; accepted for publication Dec. 7, 1997.)

ABSTRACT

By applying linear perturbation theory to the radiation transport equation, the inverse problem of optical diffusion tomography can be reduced to a set of linear equations, $\mathbf{W}\boldsymbol{\mu}=\mathbf{R}$, where $\mathbf{W}$ is the weight function, $\boldsymbol{\mu}$ are the cross-section perturbations to be imaged, and $\mathbf{R}$ is the detector readings perturbations. We have studied the dependence of image quality on added systematic error and/or random noise in $\mathbf{W}$ and $\mathbf{R}$. Tomographic data were collected from cylindrical phantoms, with and without added inclusions, using Monte Carlo methods. Image reconstruction was accomplished using a constrained conjugate gradient descent method. Results show that accurate images containing few artifacts are obtained when $\mathbf{W}$ is derived from a reference state whose optical thickness matches that of the unknown test medium. Comparable image quality was also obtained for unmatched $\mathbf{W}$, but the location of the target becomes more inaccurate as the mismatch increases. Results of the noise study show that image quality is much more sensitive to noise in $\mathbf{W}$ than in $\mathbf{R}$, and the impact of noise increases with the number of iterations. Images reconstructed after pure noise was substituted for $\mathbf{R}$ consistently contain large peaks clustered about the cylinder axis, which was an initially unexpected structure. In other words, random input produces a nonrandom output. This finding suggests that algorithms sensitive to the evolution of this feature could be developed to suppress noise effects.
 [S1083-3668(98)00902-2]

Keywords optical diffusion tomography; image reconstruction; inverse problem; image quality.

1 INTRODUCTION

There has been sufficiently extensive development of optical diffusion tomography in recent years so that some applications are ready for clinical testing.[1] Two types of tomographic schemes have been used. In cross-section imaging, first proposed by our group and later also adopted by many other teams,[2] one tries to map the perturbations of physical properties such as the scattering and absorption cross sections relative to a reference state, as a function of physiological or pathological conditions, e.g., oxygenation/deoxygenation of hemoglobin and myoglobin,[3] brain hemorrhage,[4] or breast cancer.[5,6] The newly developed luminescence imaging[7,8] uses a similar idea, by assuming that the presence of fluorophore/phosphor slightly perturbs the background absorption cross sections. In addition, it takes advantage of the difference between the excitation and emission spectra in the phenomena of fluorescence or phosphorescence in order to image the fluorophore/phosphor concentration and mean lifetime as a function of physiological or pathological condition. In either case, the inverse problem reduces to a system of linear equations[7–9] having the form $\mathbf{W}\boldsymbol{\mu}=\mathbf{R}$ when it is based on a perturbed transport equation. Here, $\mathbf{W}$ is the weight matrix, whose elements are proportional to products of forward (from source to voxel) and adjoint (from voxel to detector) intensities; $\boldsymbol{\mu}$ is the quantity to be imaged; and $\mathbf{R}$ is the detector readings.

Because both imaging techniques employ perturbation methods, the quality of reconstructed images is a function of modeling error, that is, the magnitude of the discrepancy between the test medium and the reference (cross section imaging) or background medium (luminescence imaging). We have studied two methods for estimating the physical properties of the reference or background medium in the (realistic) case in which they are not known *a priori*. In the first,[10] one begins with a simple preselected medium, typically in a homogeneous state, and repeatedly alternates between solving the perturbation equation for $\boldsymbol{\mu}$ and computing a new $\mathbf{W}$ based on the current estimate of $\boldsymbol{\mu}$. This is similar to the iterative Born approximation used in microwave imaging[11] and is usually very computation

Address all correspondence to Jenghwa Chang, Memorial Sloan-Kettering Cancer Center, Dept. of Medical Physics, 1275 York Ave., New York, NY 10021; Tel: (212) 639-6036; Fax: (212) 717-3010; E-mail: chang_jenghwa@mskcc.org

1083-3668/98/$10.00 © 1998 SPIE

intensive because multiple forward calculations are needed to update the weight matrix. The second method[5,6] assigns the average physical properties of the various tissue types known to be present in a given sample to an anatomically accurate map obtained from some other imaging modality, e.g., CT or MRI. This requires image segmentation and registration techniques to process the anatomical images, but these are generally much faster than updating the forward calculation. In the best case, a single step of solving the forward and inverse problems would suffice. If it should still prove necessary in practice to repeat the process, the number of iterations required would be smaller under this approach than by starting from an assumption of homogeneity. The probability of the iterative process diverging would likewise be smaller.

The quality of reconstructed images in optical tomography is affected by modeling error and by noise in the detected signals. Two types of modeling error may occur. The first is systematic error or systematic mismatch, by which we mean the error introduced by either overestimating or underestimating the optical thickness of the test medium. An example would be that the initial guess is a homogeneous medium whose cross sections are systematically larger or smaller than those of the test medium. Errors of this type could be expected to occur if, for example, the reference medium is selected in the absence of sufficient *a priori* knowledge of the target medium or if optical cross section estimates are assigned to pixels in an anatomical image of the target medium on the basis of inaccurate literature values. The second type of modeling error is random mismatch, which refers to discrepancies between the reference and test media when they are close to each other after a few steps of multistep reconstruction, or that could be expected if the reference medium is derived from an anatomically accurate map and the assigned literature values are accurate, or that arise from positioning uncertainty as described by Boas et al.[12] The random mismatch is typically much smaller than the systematic mismatch and can be modeled as multiplicative noise. Realistic noise levels for the random mismatch caused by positioning error are at least 2% in amplitude and 0.3° in phase.[12]

Previous studies[13,14] have shown that **W** is an ill-conditioned matrix; thus, the reconstructed result is very sensitive to noise in the detector readings. In general, two types of noise are encountered in an optical imaging system.[15] The first is shot (Poisson) noise due to statistical variations inherent in the mechanisms of photon generation and interaction with the target medium. Its magnitude is proportional to the square root of the detected photon count, and it can be reduced by increasing either the source intensity or the detector acquisition time.[15] The second is independent additive noise that manifests as dark current in the counter and electronics, and also arises as a consequence of numerical errors (e.g., quantization error). Its effect can be lessened by proper filtering.[15]

One way to overcome ill conditioning is to apply constraints derived from *a priori* knowledge of the target medium to the image reconstruction. This will help confine the results within a feasible range and avoid meaningless reconstructions. The disadvantage of imposing constraints is that it leads to a nonlinear solution to a set of linear equations, i.e., the image recovered from a linear combination of two sets of detector readings is not equal to the corresponding linear combination of the individual images. The techniques currently in use by ours and other groups do not necessarily require *a priori* information.[16,17] However, as demonstrated in this paper and other studies[6,10] it is better to use it when some is available.

Studies by Moon et al.[18,19] used analytic expressions for diffusing light to determine the achievable resolution for imaging through turbid media. In this work, the half-width of the point spread function of a single source was calculated for media of different optical thicknesses, and it was found that image resolution degraded linearly with the sample thickness with a scale dependence of $R(d) \approx 0.2d$, where R is the achievable resolution and d is the sample thickness. They also point out that tomographic reconstruction may improve this limit because multiple sources and detectors are used. More recently, Boas et al.[12] performed an extensive study of detection limits for multiple sources and detectors, by analyzing different moments of the diffuse photon density waves and comparing them to the uncertainties caused by shot noise and positioning error. They concluded that the determination of size and optical properties is a function of the optical cross sections of the background and target media and of the modulation frequency. Simultaneous determination of size and geometry can be achieved for an inhomogeneity with diameter on the order of 1.0 cm or larger, and if there is *a priori* information about either the object's size or optical properties, the remaining unknown quantities can be determined for diameters as small as 0.3 cm. This last conclusion is consistent with Moon's results.

In this paper, we expand upon results of an earlier study originally presented in the 1995 IEEE Nuclear Science Symposium and Medical Image Conference.[20] Unlike the studies cited above, which looked for the detection limits, the purpose of this study is to focus on the impact of modeling error and random noise on reconstructed images. Here, one-step reconstructed images of simple phantoms, using detector readings generated by Monte Carlo simulations and a previously developed constrained conjugate gradient descent algorithm, are used to illustrate the dependence of image quality on systematic errors in the imaging operator and on noise. Systematic mismatches were introduced in the weight matrices by reconstructing images of a

simply-structured phantom medium using weight matrices for reference media with different optical thicknesses, and random mismatches were modeled by adding multiplicative noise at different levels to each element of the weight matrix. Random Gaussian noise at different levels was added to the detector readings to examine its effect on the reconstructed images. The effect of positivity constraints on the reconstruction of noisy data is taken up again in the Discussion.

2 THEORY

The inverse problems for absorption cross section imaging and fluorescence imaging reduce to systems of linear equations:

$$\mathbf{W}\boldsymbol{\mu}=\mathbf{R}, \tag{1}$$

where $\mathbf{W}$ is the weight matrix, $\boldsymbol{\mu}$ is the vector of unknown absorption cross section perturbations or of products of fluorophore concentration and quantum yield, and $\mathbf{R}$ is the vector of detector readings (luminescence imaging) or detector readings perturbations (cross section imaging). In absorption cross section imaging,[9] Eq. (1) is a discretized version of an integral equation:

$$\Delta R=\int_V w_a \Delta\mu_a d^3r, \tag{2}$$

where $\Delta\mu_a$ is the macroscopic absorption cross section perturbation (mm^{-1}), ΔR is the detector reading perturbation, and w_a is the weight function:

$$w_a=-(\phi_0\phi_0^+-3\mathbf{J}\cdot\mathbf{J}^+)/4\pi, \tag{3}$$

where

$$\phi_0=\int_{4\pi}\phi d\Omega, \quad \mathbf{J}=\int_{4\pi}\phi\Omega d\Omega,$$

$$\phi_0^+=\int_{4\pi}\phi^+ d\Omega, \quad \mathbf{J}^+=-\int_{4\pi}\phi^+\Omega d\Omega,$$

and ϕ and ϕ^+ are forward (from a source to a voxel) and adjoint (from a voxel to a detector) angular intensities, obtained by solving a transport equation.[9] In the fluorescence imaging case,[7] Eq. (1) is a discretized version of

$$R=\int_V w_{fl}(\gamma N_0)d^3r, \tag{4}$$

where R is the emitted fluorescence intensity, γ is the quantum yield, N_0 is the fluorophore concentration, and

$$w_{fl}=\Sigma_{T,1\to2}\phi_0^1\phi_0^{2+}/4\pi, \tag{5}$$

where $\Sigma_{T,1\to2}$ is the microscopic total cross section (mm^2) introduced by the fluorophore, and ϕ_0^1 and ϕ_0^{2+} are, respectively, the forward and adjoint integrated intensities of the exciting and emitted light. Because $\mathbf{J}\cdot\mathbf{J}^+$ is usually much smaller than $\phi_0\phi_0^+$, w_a for the absorption cross section imaging problem can be well approximated by including only the first term in the numerator of Eq. (3). In this sense, the weight matrix in both the absorption cross section imaging and fluorescence imaging cases are essentially the same, and the findings of studies of one imaging modality will also apply for the other.

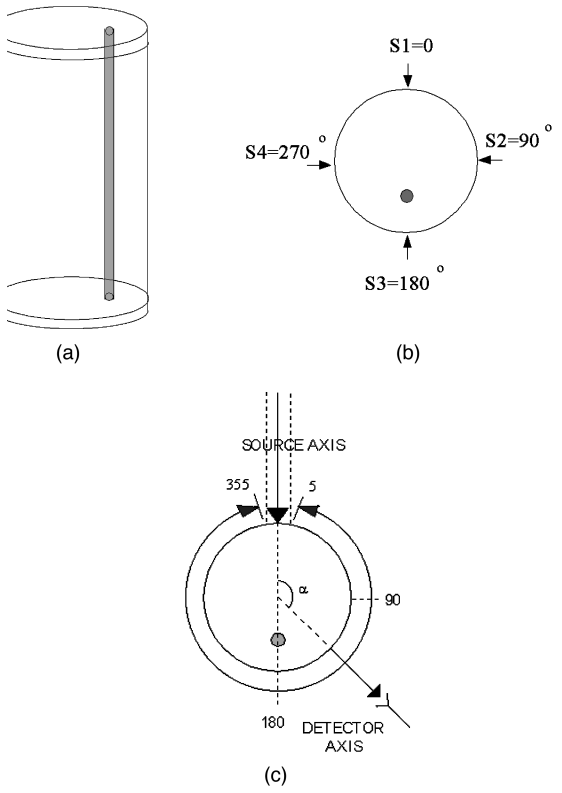

Fig. 1 (A) Tissue phantom modeled in Monte Carlo simulations. (B) Source configuration. (C) Simulation detector configuration for each source. The detectors were located every 10° about the boundary of the phantom.

3 METHODS

3.1 MONTE CARLO SIMULATION

Two sources of error were introduced in this study. The first was a systematic error, produced by varying the total cross section ($\boldsymbol{\mu}_T=\boldsymbol{\mu}_a+\boldsymbol{\mu}_s$) of the reference medium. The second, random error, is described below in Sec. 3.3. Monte Carlo simulations (MCS) modeled continuous-wave (cw) light propagation in a cylindrical phantom of 20 mean free paths (mfp) diameter, as shown in Figure 1, with and without a black absorber at an off-axis location. The absorber was a cylindrical inhomogeneity (i.e., a rod) of 1 mfp diameter located halfway between the axis and the boundary of the cylinder. The pho-

ton scattering was isotropic. The perturbed detector readings, **R**, were obtained by calculating the differences, at all detector locations, between the detected intensities in the absence and presence of the black rod. The matched weight matrix **W** was calculated from the forward and adjoint collision densities in each voxel. The simulated **R** and **W** are essentially noiseless except for Poisson noise arising from the MCS, which is minimal since $O(10^8)$ photons were simulated and the correlated sampling was used for variance reduction. MCS was also performed to get unmatched weight matrices from media of 10, 40, and 100 mfp diameter. This is equivalent to varying the total cross section, $\boldsymbol{\mu}_T$, while keeping the physical dimensions of the phantom constant. The matched and unmatched matrices were also used for image reconstruction from experimental data.

3.2 NOISE

To study the effect of random error, different levels of Gaussian white noise were produced by a random number generator.[21] The generated noise was then added to the detector readings

$$R_i' = R_i + n_i, \tag{6}$$

where R_i is the ith detector reading, n_i is the noise, R_i' is the noise-added detector reading, and the noise level is defined as

$$\text{noise level } (\%) = 100\,\frac{\text{noise variance}}{\text{average signal power}}. \tag{7}$$

Noise was also added to the weight function

$$w_{ij}' = (1 + n_{ij}) w_{ij}, \tag{8}$$

where w_{ij}' is the noise-added element of the weight matrix, and the noise level is defined as

$$\text{noise level } (\%) = 100 \cdot (\text{noise variance}). \tag{9}$$

The levels of noise added to the detector readings were 1%, 5%, 10%, 50%, 100%, and 500%, while the levels of noise added to the weight function were 1%, 5%, 10%, 50%, and 100%. To comply with the physical necessity that the weight function be nonnegative for absorption cross section perturbations, any negative noise-added weight matrix elements were set to zero. The detector readings and weight matrices were then used for image reconstruction and the reconstructed images were compared to the results with no added noise. As a control, reconstructions were also performed using only generated Gaussian white noise as the detector readings, and the noise-free matched weight matrix.

3.3 RECONSTRUCTION ALGORITHM

A previously developed constrained conjugate gradient descent (CGD) algorithm with a rescaling technique[22] was used for image reconstruction. The CGD method iteratively updates the reconstruction on the basis of the previous reconstruction and all the preceding gradient and conjugate gradient vectors:

$$\boldsymbol{\mu}^n = \boldsymbol{\mu}^{n-1} - \alpha^n \mathbf{d}^n, \tag{10}$$

where

$$\alpha^n = \frac{(\mathbf{g}^{n-1})^T \mathbf{g}^{n-1}}{(\mathbf{d}^n)^T \mathbf{A} \mathbf{d}^n}, \quad \mathbf{d}^n = -\mathbf{g}^{n-1} + \beta^n \mathbf{d}^{n-1},$$

$$\beta^n = \frac{\|\mathbf{g}^{n-1}\|^2}{\|\mathbf{g}^{n-2}\|^2}, \quad \mathbf{g}^n = \mathbf{A}\boldsymbol{\mu}^n - \mathbf{b} = \mathbf{g}^{n-1} - \alpha^n \mathbf{A}\mathbf{d}^n,$$

$$\mathbf{g}^0 = \mathbf{A}\boldsymbol{\mu}^0 - \mathbf{b}, \quad \mathbf{d}^1 = -\mathbf{g}^0, \quad \beta^1 = 0,$$

where $\mathbf{A} = \mathbf{W}^T\mathbf{W}$, $\mathbf{b} = \mathbf{W}^T\mathbf{R}$, $\boldsymbol{\mu}^0$ is the initial guess, $\mathbf{g}^n$ is the gradient vector and $\mathbf{d}^n$ is the conjugate gradient vector. Range constraints on the **R** were imposed prior to reconstruction, with all the negative readings set to zero:

$$\Delta R_i = \max(\Delta R_i, 0), \tag{11}$$

where ΔR_i is the ith component of **R**. Range constraints were imposed on reconstruction results after each iteration:

$$\Delta \mu_j^n = \max(\Delta \mu_j^n, 0), \tag{12}$$

where $\Delta \mu_j^n$ is the jth component of $\boldsymbol{\mu}^n$. Applying positivity constraints to the previous reconstruction, $\boldsymbol{\mu}^{n-1}$, leads to miscalculation of $\mathbf{g}^n$ and $\mathbf{d}^n$, and this can cause the algorithm to diverge. To overcome this difficulty, the following divergence detection scheme was devised. Let the ratio of two consecutive mean squared errors be

$$r^n = \frac{E^n}{E^{n-1}}, \tag{13}$$

where $E = \frac{1}{2}\boldsymbol{\mu}^T\mathbf{A}\boldsymbol{\mu} - \mathbf{b}^T\boldsymbol{\mu} + \frac{1}{2}\mathbf{R}^T\mathbf{R}$ is the mean squared error. The reconstruction result will diverge if $r^n > 1$ for any n. Once this happens, the conjugate gradient vector is reset, i.e., $\mathbf{d}^n = \mathbf{0}$, and the CGD reconstruction is restarted using the previous reconstruction result, $\boldsymbol{\mu}^{n-1}$, as the initial value.

A rescaling technique, which sets the maximum value of each column of the weight matrix **W** to 1.0 exactly, i.e., $w_{ij}' = w_{ij} / \max_{i=1}^{I}\{w_{ij}\}$, to make **W** more uniform and possibly better conditioned, was used to suppress numerical errors and accelerate convergence.[22]

4 RESULTS

Figure 2 shows the images reconstructed from MCS-generated data without added noise, using the matched weight matrix and the CGD method, after 1000 iterations. Figure 2(A) is the target image;

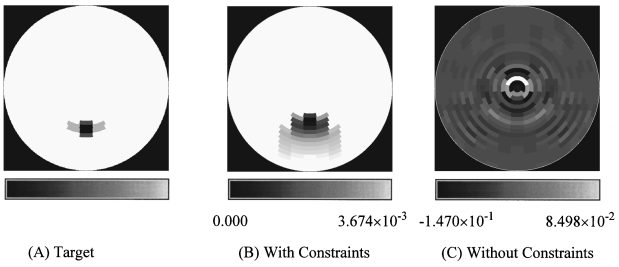

Fig. 2 Images reconstructed from simulation data, after 1000 iterations without added noise, with matched weight matrix, using the CGD method with (B) and without (C) positivity constraints. (A) is the target image.

Figure 2(B) is the image reconstructed with positivity constraints; and Figure 2(C) is the result obtained without use of constraints. Figures 3(A)–3(C) show the reconstructed images obtained by using unmatched weight matrices for media of 10, 40, and 100 mfp diameter, respectively.

The images reconstructed from simulation data with 5%, 10%, 100%, and 500% white noise added to the detector readings are shown in Figure 4. The reconstruction results for the 10% added noise case after 10, 100, and 1000 iterations are shown in Figure 5. The results for the noise-free detector readings with 5%, 10%, and 100% white noise added to the matched weight matrix are shown in Figure 6, and the reconstructed images for the 100% noise case after 10, 100, and 1000 iterations are shown in Figure 7. Reconstruction results from the simulation data with 5%, 10%, and 100% added white noise in both the detector readings and weight matrices are shown in Figure 8. Figure 9 shows the results from the pure noise data after 100 iterations, using the CGD method without constraints, where the indicated 1%, 10%, and 100% noise levels are the same as those added to the detector readings. In these results, the most positive and most negative image values both lie in voxels near the cylinder axis. Figure 10 shows the analogous results using the constrained CGD method.

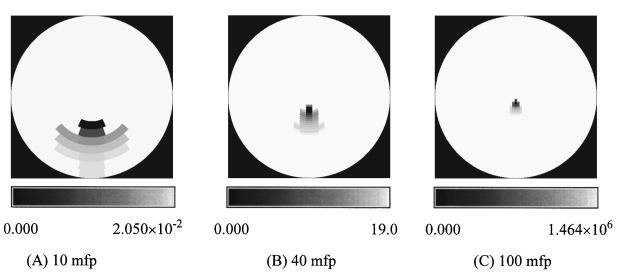

Fig. 3 Images reconstructed from simulation data, after 1000 iterations of the CGD method, with unmatched weight matrices. The target is the same as shown in Figure 2(A).

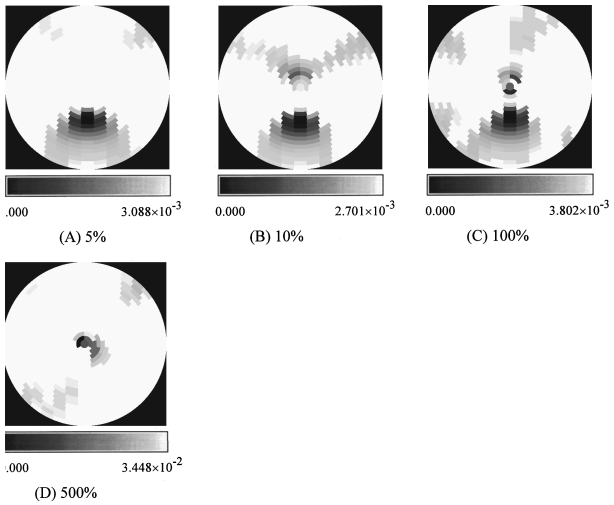

Fig. 4 Images reconstructed from simulated detector readings with additive Gaussian white noise after 100 iterations. Noise levels are: (A) 5%, (B) 10%, (C) 100%, and (D) 500%. The target is the same as shown in Figure 2(A).

5 DISCUSSION AND CONCLUSIONS

Currently applicable image reconstruction schemes in optical tomography require *a priori* knowledge of the physical properties of the reference or background medium, which frequently is difficult to obtain. The use of other image modalities, e.g., CT or MR, provides a convenient way to estimate the physical properties but introduces a mismatch in the weight matrices. Our analysis of a simply structured phantom shows that qualitatively good (i.e., few artifacts, size and shape of image peak nearly correct, sharp edge detection) images [Figure 2(B)] can be obtained and the rod can be accurately located using the constrained CGD method, when the reconstruction is based on noiseless detector readings and the matched weight matrix. The same data and reconstruction algorithm yielded unacceptable results [Figure 2(C)] when positivity constraints were not used. This strongly suggests that even if the use of constraints in reconstruction may lead to a nonlinear solution to a set of linear equations, the advantage confers by restricting the reconstructed results to a feasible and interpretable region more

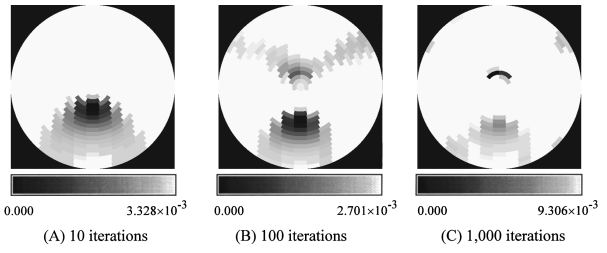

Fig. 5 Images reconstructed from simulation data with 10% Gaussian white noise added to the detector readings after (A) 10 iterations, (B) 100 iterations, and (C) 1000 iterations. The target is the same as shown in Figure 2(A).

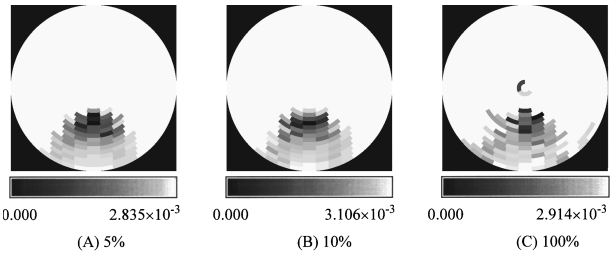

Fig. 6 Images reconstructed from simulation data with noise added to the weight matrix, after 1000 iterations. Noise levels are: (A) 5%, (B) 10%, (C) 100%. The target is the same as shown in Figure 2(A).

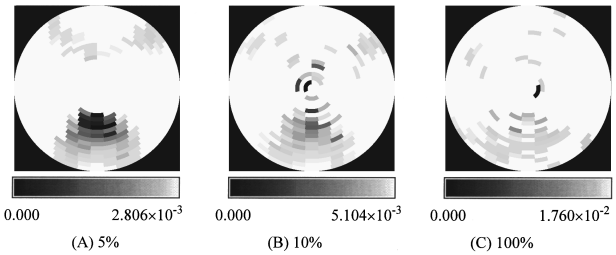

Fig. 8 Images reconstructed from simulation data with noise added to both the detector readings and the weight matrix, after 100 iterations. Noise levels are: (A) 5%, (B) 10%, (C) 100%. The target image is the same as shown in Figure 2(A).

than compensates. Good image quality was also obtained for unmatched weight matrices [Figures 3(A)–3(C)], but the location of the rod in the image becomes increasingly inaccurate as the mismatch increases.

The noise study shows that the reconstruction algorithm is much more sensitive to noise in the weight matrix than to noise in the detector readings, when compared to the reconstructed results with no added noise [Figure 2(B)]. The structure of the rod can be identified with reasonable accuracy with as much as 100% noise [noise variance equals power of detector readings; Figures 4(A)–4(C)] added to the detector reading, but 5% [Figures 6(A)–6(C)] noise added to the weight matrix is sufficient to blur the rod structure. However, an encouraging finding is that the rod location remains accurate with as much as 100% noise added to the weight matrix [Figure 6(C)]. This indicates that if we are interested only in detecting the presence and specifying the location of an inhomogeneity, and not so much in characterizing its structure, a rough estimate of the weight matrix from an anatomically accurate map is good enough to produce acceptable results. However, when the same amount of noise is added to both detector readings and the weight matrix, the combined effect may reduce the image quality dramatically with as little as 10% added noise (compare Figures 4, 6, and 8).

The impact of noise on an image increases with the number of iterations of the reconstruction algorithm when noise is added to the detector readings (Figure 5). A similar phenomenon (not shown) was also observed in images reconstructed using the SART algorithm, which, like CGD, is a simultaneous iterative reconstruction algorithm, but was not observed when the (sequential, iterative) POCS method was used. There is a plausible, testable explanation for these phenomena. When noise is added to the detector readings, we can conveniently consider the reconstructed image as a sum of a noiseless detector readings image and a pure noise image (this is not strictly true, because the positivity constraints imposed on the reconstruction results make the inverse problem nonlinear). Because noise is randomly added to the detector readings, it is evenly distributed in all dimensions of the detector readings space. The CGD algorithm updates voxels by moving the evolving solution in the direction of the conjugate gradient, and those voxels with the highest weights will be affected by noise in earlier iterations due to their greater contributions to the conjugate gradient. Thus, the spatial extent of the noise effect seen in early stages of the reconstruction is quite limited, and the magnitude of the effect is much smaller than that of the noiseless detector readings [Figure 5(A)]. As the number of iterations increases, the noise effect spreads out over the entire volume involved in the reconstruction and finally dominates the results [Figure 5(C)]. There is not such a clear trend, however, when noise is added to the weight matrix (Figure 7). In comparison to the results obtained with systematically mismatched weight matrices

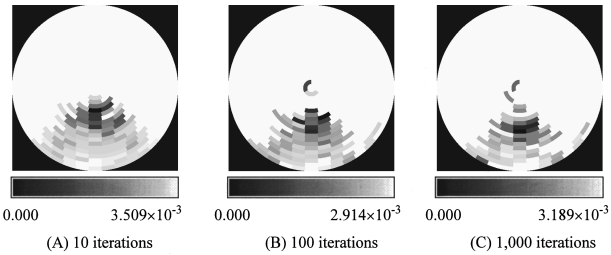

Fig. 7 Images reconstructed from simulation data with 100% noise added to the weight matrix after (A) 10 iterations, (B) 100 iterations, and (C) 1000 iterations. The target is the same as shown in Figure 2(A).

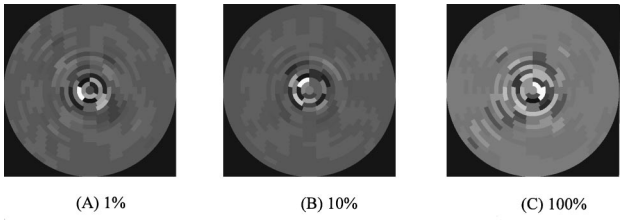

Fig. 9 Images reconstructed from pure noise data as the detector readings, using the CGD method without positivity constraint: (A) 1%, (B) 10%, (C) 100%, after 100 iterations. The most negative (white) and most positive (black) image values both occur in voxels lying near the cylinder axis.

Fig. 10 Image reconstructed from pure noise data as the detector readings, using the constrained CGD method, after 100 iterations. Noise levels are: (A) 1%, (B) 10%, (C) 100%.

(Figures 2 and 3), the randomly mismatched weight matrices cause more structural change than position change in the reconstructed images (Figure 7).

The ''images'' obtained when pure noise (Figures 9 and 10) was substituted for **R** have an initially unexpected nonrandom structure, with the greatest absolute image intensity in voxels near the cylinder axis. This is unlike other image modalities such as CT and MRI, where images that are uniformly zero±random noise sprinkled throughout would be expected under such reconstruction conditions. One possible explanation is that this phenomenon is caused by the nonlinearity arising from our use of positivity constraints, but this is ruled out by the observation that it occurs as well when the reconstruction is unconstrained. The results are, on the other hand, consistent with the ill-conditioned structure of the weight matrix, whose columns representing voxels near the axis contain much smaller elements than those in columns corresponding to peripheral voxels. Nevertheless, the effect of random input is to produce a nonrandom output. Moreover, as seen in Figures 6 and 7, the path to this result also appears to be structured (i.e., the image evolves towards the center). This observation may lend itself to the development of algorithms which seek to detect trends in the evolving image that are consistent with the effect of added noise and adaptively filter out this effect.

5.1 IMPACT ON MEDICAL IMAGING

This study demonstrates the effect of mismatched weight matrices and noise on image reconstruction in optical diffusion tomography. When applying optical diffusion tomography to diagnostic medical imaging for detecting, say, a tumor or hemorrhage, a weight matrix mismatch could be expected to arise from positioning uncertainty and from the discrepancy between the real reference medium and the one obtained either from an anatomically accurate map from other image modality or from the iterative Born approximation. The sources of noise in the detected signal are shot noise, environmental dark current, and numerical errors. Our results demonstrate that our reconstruction algorithm is more sensitive to mismatches in the weight matrix than to noise in the detector readings. The major factors determining the accuracy of the weight matrix are the tissue scattering and absorption cross sections and the photon transport model. Currently available cross section data are incomplete and insufficient to characterize different tissue types. Even for a single tissue type (e.g., breast tissue), significant discrepancies are observed among different reported values because of different modeling and measurement schemes. In terms of photon transport models, the diffusion approximation to the transport equation has long been used as a standard approach for photon transport because it is relatively simple in comparison to the transport equation and its solutions are in good agreement with experimental data for special cases such as infinite uniform media. However, a study by Hielscher et al.[23] has shown that the discrepancy between solutions of the transport and diffusion equations may be as high as 100% in a finite, inhomogeneous medium. In addition, some reports point out that even the transport equation may not accurately model photon transport because it does not consider interference and other wave phenomena. Thus, without more accurate tissue data and photon transport models, the application of diffuse optical tomography may be limited to phantom studies or to tissues that are uniform and well characterized, such as breast tissue.

Although image quality is less sensitive to noise in the detector readings than in the weight function, an effort should still be made to reduce its influence to the lowest level. Shot noise can be reduced by increasing the source intensity and/or increasing the signal acquisition time. Care should be taken to make sure that the source intensity is within the tissue tolerance limits, and patient immobilization is important to reduce the positioning uncertainty caused by increasing the integration time. The effects of dark current and numerical error can be reduced by better equipment setup and proper filtering (e.g., incorporating regularization[24] and total least squares[25] techniques to enhance image quality). In addition, our study suggests that when gradient-type reconstruction algorithms are used, a compromise between image quality and noise effects should be considered when choosing the number of iterations. This is in contrast to the case of ideal, noiseless data, where the reconstruction typically improves steadily as the number of iterations is increased.

Acknowledgment

This work was supported in part by NIH Grant R01 CA59955 and by NIH Grant R01 CA66184.

REFERENCES

1. *Optical Tomography, Photon Migration, and Spectroscopy of Tissue and Model Media: Theory, Human Studies, and Instrumentation,* B. Chance and R. R. Alfano, Eds., *Proc. SPIE* **2389** (Feb. 1995).
2. *Medical Optical Tomography: Functional Imaging and Monitoring*, G. Müller et al., Eds., *SPIE Institutes*, Vol. IS11, SPIE Press, Bellingham, WA (1993).

3. B. Chance, ''Optical method,'' in *Annu. Rev. Biophys. Biophys. Chem.* **20**, 1–28 (1991).
4. D. A. Benaron, J. P. Van Houten, W.-F. Cheong, E. L. Kermit, and R. A. King, ''Early clinical results of time-of-flight optical tomography in a neonatal intensive care unit,'' in *Proc. Optical Tomography, Photon Migration, and Spectroscopy of Tissue and Model Media: Theory, Human Studies, and Instrumentation, Proc. SPIE* **2389**, 448–464 (Feb. 1995).
5. J. Chang, H. L. Graber, and R. L. Barbour, ''Progress toward optical mammography: imaging in dense scattering media using time-independent optical sources,'' in *1994 IEEE Conference Record of Nuclear Science Symposium and Medical Imaging Conference*, pp. 1484–1488, Norfolk, VA (Nov. 1994).
6. R. L. Barbour, S. S. Barbour, P. C. Koo, H. L. Graber, R. Aronson, and J. Chang, ''MRI-guided optical tomography,'' *IEEE Comput. Sci. Eng. Mag.* **2**(4), 63–77 (1995).
7. J. Chang, R. L. Barbour, H. Graber, and R. Aronson, ''Fluorescence optical tomography,'' in *Proc. Experimental and Numerical Methods for Solving Ill-Posed Inverse Problems: Medical and Nonmedical Applications, Proc. SPIE* **2570**, 59–72 (1995).
8. M. A. O'Leary, D. A. Boas, X. D. Li, B. Chance, and A. G. Yodh, ''Fluorescence lifetime imaging in turbid media,'' *Opt. Lett.* **21**, 158–160 (1996).
9. J. Chang, R. Aronson, H. L. Graber, and R. L. Barbour, ''Imaging diffusive media using time-independent and time-harmonic sources: Dependence of image quality on imaging algorithms, target volume, weight matrix, and view angles,'' in *Proc. Optical Tomography, Photon Migration, and Spectroscopy of Tissue and Model Media: Theory, Human Studies, and Instrumentation, Proc. SPIE* **2389**, 448–464 (Feb. 1995).
10. S. R. Arridge and M. Schweiger, ''Sensitivity to prior knowledge in optical tomographic reconstruction,'' in *Proc. Optical Tomography, Photon Migration, and Spectroscopy of Tissue and Model Media: Theory, Human Studies, and Instrumentation, Proc. SPIE* **2389**, 378–388 (Feb. 1995).
11. W. C. Chew and Y. M. Wang, ''Reconstruction of two-dimensional permittivity distribution using the distorted Born iterative method,'' *IEEE Trans. Med. Imag.* **9**, 218–225 (1990).
12. D. A. Boas, M. A. O'Leary, B. Chance, and A. G. Yodh, ''Detection and characterization of optical inhomogeneities with diffuse photon density waves: A signal-to-noise analysis,'' *Appl. Opt.* **36**, 75–92 (1997).
13. J. Chang, Y. Wang, R. Aronson, H. L. Graber, and R. L. Barbour, ''A layer stripping approach for recovery of scattering medium using time-resolved data,'' *Proc. SPIE* **1767**, **384–395** (July 1992).
14. S. R. Arridge, M. Schweiger, and D. T. Delpy, ''Iterative reconstruction of near infrared absorption images,'' *Proc. SPIE* **1767**, 372–383 (July 1992).
15. A. G. Marshall and F. R. Verdun, *Fourier Transforms in NMR, Optical, and Mass Spectrometry*, Chap. 5, Elsevier Science Publishing, New York (1990).
16. D. Y. Paithankar, A. Chen, and E. M. Sevick-Muraca, ''Fluorescence yield and lifetime imaging in tissues and other scattering media,'' *Proc. SPIE* **2679**, 162–175 (1996).
17. H. Jiang, K. D. Paulsen, U. L. Österberg, and M. S. Patterson, ''Frequency-domain optical image reconstruction in turbid media: An experimental study of single-target detectability,'' *Appl. Opt.* **36**, 52–63 (1997).
18. J. A. Moon, R. Mahon, M. D. Ducan, and J. Reintjes, ''Resolution limits for imaging through turbid media with diffuse light,'' *Opt. Lett.* **18**, 1591–1593 (1993).
19. J. A. Moon and J. Reintjes, ''Image resolution by use of multiply scattered light,'' *Opt. Lett.* **19**, 521–523 (1994).
20. J. Chang, H. L. Graber, and R. L. Barbour, ''Dependence of optical diffusion tomography image quality on image operator and noise,'' in *1995 IEEE Conference Record of Nuclear Science Symposium and Medical Imaging Conference*, pp. 1524–1528, San Francisco, California (Oct. 1995).
21. W. H. Press, S. A. Teukolsky, W. T. Vetterling, and B. P. Flannery, *Numerical Recipes in FORTRAN*, 2nd ed., Cambridge University Press, Cambridge, England (1992).
22. J. Chang, H. L. Graber, and R. L. Barbour, ''Image reconstruction of dense scattering media from CW sources using constrained CGD and a matrix rescaling technique,'' in *Proc. Optical Tomography, Photon Migration, and Spectroscopy of Tissue and Model Media: Theory, Human Studies, and Instrumentation, Proc. SPIE* **2389**, 448–464 (Feb. 1995).
23. A. H. Hielscher, R. E. Alcouffe, and R. L. Barbour, ''Transport and diffusion calculations on MRI-generated data,'' in *Proc. Optical Tomography and Spectroscopy of Tissue: Theory, Instrumentation, Model, and Human Studies, Proc. SPIE* **2979**, 500–508 (Feb. 1997).
24. W. Zhu, Y. Wang, H. L. Graber, R. L. Barbour, and J. Chang, ''A regularized progressive expansion algorithm for recovery of scattering media from time-resolved data,'' *OSA Proceedings on Advances in Optical Imaging and Photon Migration*, Vol. 21, pp. 211–216, Orlando, Florida (Mar. 1994).
25. W. Z. Zhu, Y. Wang, J. Chang, H. L. Graber, and R. L. Barbour, ''Image reconstruction in scattering media from time-independent data: A total least squares approach,'' in *Proc. Optical Tomography, Photon Migration, and Spectroscopy of Tissue and Model Media: Theory, Human Studies, and Instrumentation, Proc. SPIE* **2389**, 420–430 (Feb. 1995).